Construction and Building Materials 535 (2026) 146925

Contents lists available at ScienceDirect

Construction and Building Materials

journal homepage: www.elsevier.com/locate/conbuildmat

An experimental investigation of multi-panel cross-laminated timber shearwalls

Mohammad Masroor [a,*], Ghasan Doudak [a], Daniele Casagrande [b]

[a] Department of Civil Engineering, University of Ottawa, Ottawa, ON K1N 6N5, Canada
[b] Department of Civil, Environmental, and Mechanical Engineering, University of Trento, Trento, Italy

ARTICLE INFO

Keywords:
Cross-laminated timber
Multi-panel Shearwalls
Experimental tests
Connections
Analytical models

ABSTRACT

This paper presents an experimental investigation on single-storey multi-panel Cross-Laminated Timber (CLT) shearwalls subjected to lateral loads. The study focuses on shearwalls with a variable number of panels and considers factors such as dead load and the relative stiffness between the panel-to-panel connections and hold-downs to achieve two distinct kinematic modes, namely Coupled-Panel (CP) and Single-Wall (SW). Twelve full-scale tests were conducted, covering two primary configurations: one in which sliding was prevented through supports, and another where sliding was resisted by angle brackets. The findings revealed that gravity load enhances shearwall resistance in both CP and SW, while having limited impact on stiffness and ductility. Walls exhibiting SW had greater stiffness but lower ultimate displacement and ductility due to the increased number of panel-to-panel connections. Increasing the panels quantity while maintaining the same shearwall length reduced resistance and stiffness, while ductility improved slightly. It was also observed that adding angle brackets resulted in enhanced resistance. Reasonable agreement was found when the experimental results were compared with the numerical model, including close alignment between observed kinematic modes and those predicted through numerical analysis. The numerical models also appropriately predicted the plastic regions, capturing yielding and local failure in the connections. Comparison between test results and analytical expressions, recently adopted in the Canadian timber design standard and forthcoming Eurocode 8, showed that the analytical expressions can adequately capture the kinematic modes and yield hierarchy with acceptable accuracy, particularly in predicting the wall's lateral strength.

1. Introduction and background

Cross-laminated timber (CLT) panels possess high in-plane strength and stiffness, which makes them ideal for use as shearwalls. When the aspect ratio of the wall segments is selected within a range that promotes rocking rather than sliding behaviour, the boundary connection can be engaged and designed such that they can control the failure mechanism and contribute to the strength, stiffness and ductility of the lateral load resisting system (LLRS). This approach has, for example, been adopted in the Canadian timber design standard CSA O86–24 [1], where the wall segment has been limited to aspect ratios between 2:1 and 4:1 for seismic deign. Although this range of aspect ratios promotes the desired rocking behaviour it does not ensure it, since the kinematic behaviour of the wall depends on the relative stiffness and yield strengths of the boundary connections (i.e., hold-downs and panel-to-panel connections). As such, the 2024 edition of CSA O86–24 [1] adopts analytical expressions for elastic strength, lateral deflection, and kinematic mode of CLT shearwalls, along with a plastic design that establishes a yield hierarchy among dissipative connections and requires over-protection of limited- and non-dissipative connections.

Previous experimental investigations on the behaviour of CLT shearwalls subjected to in-plane lateral loading have confirmed that the wall assembly exhibits rigid-body behaviour in the CLT panels, while deformation is principally achieved in the connections (e.g., [2,3]). Such connections consist of panel-to-panel joints that connect the individual CLT panels together, hold-downs, which are typically placed at the ends of the shearwall or openings to resist the uplift force, and angle brackets with the capability to resist the shear force being transmitted from the wall to the foundation or floor below (Fig. 1).

Two CLT shearwall configurations can be identified, namely single-panel and multi-panel, as shown in Fig. 1-a and Fig. 1-b, respectively. In the case of multi-panel shearwalls, the CLT panels are attached together using panel-to-panel connections, which, when engaged, are

* Corresponding author.
E-mail addresses: mmasoor@uottawa.ca (M. Masroor), gdoudak@uottawa.ca (G. Doudak), daniele.casagrande@unitn.it (D. Casagrande).

https://doi.org/10.1016/j.conbuildmat.2026.146925
Received 20 June 2025; Received in revised form 27 April 2026; Accepted 28 May 2026
Available online 6 June 2026
0950-0618/© 2026 The Authors. Published by Elsevier Ltd. This is an open access article under the CC BY-NC license (http://creativecommons.org/licenses/by-nc/4.0/).

Abbreviation/Symbols

CLT	Cross-Laminated Timber
CP	Coupled-Panel
EEEP	Equivalent Energy Elastic-Plastic
IN	Intermediate
LLRS	Lateral Load Resisting System
STS	Self-Tapping Screws
SW	Single-Wall
b	Length of each panel
B	Total length of the wall
$D_{m,EEEP}$	Ductility ratio as per the EEEP simulation
$D_{m,tri}$	Ductility ratio as per the trilinear curve
E_0	Longitudinal CLT layers modulus of elasticity
E_{90}	Transverse CLT layers modulus of elasticity
$E_{eff,1}$	Effective moduli along the horizontal direction of the CLT panels
$E_{eff,2}$	Effective moduli along the vertical direction of the CLT panels
EI_{eff}	Effective elastic bending stiffness of the CLT panels
$F_{\max}$	Maximum force
F_{sp}	Specified (unfactored) lateral load
$F_{y,EEEP}$	Yield force as per the EEEP simulation
$F_{y,tri}$	Yield force as per the trilinear curve
G_0	Longitudinal CLT layers shear modulus of elasticity
G_{eff}	Effective in-plane shear moduli of CLT wall panels
h	Height of each panel
$\widetilde{k}$	Dimensionless stiffness factor
$k_{e,EEEP}$	Elastic stiffness as per the EEEP simulation
$k_{e,tri}$	Elastic stiffness as per the trilinear curve
k_f	Elastic shear stiffness of the panel-to-panel connections
k_h	Elastic uplift stiffnesses of the hold-down
k_{sx}	Elastic shear stiffness of a single bracket
k_{sz}	Elastic uplift stiffness of a single bracket
k_A	CLT shearwall stiffnesses due to wall panel shear deformation
k_B	CLT shearwall stiffnesses due to wall panel bending deformation
k_R	CLT shearwall stiffnesses due to rocking deformation
$k_{R,b}$	Wall rocking stiffness with zero panel-to-panel connection stiffness
$k_{R,B}$	Wall rocking stiffness with rigid panel-to-panel connections
k_R'	Equivalent hold-down stiffness for CP behaviour
k_S	CLT shearwall stiffnesses due to sliding deformation
K_U	Uplift contribution factor
k_W	Equivalent lateral stiffness of the CLT shearwall
m	Number of panels
M_{sr}	Factored rocking moment resistance of the shearwall under seismic
n_f	Number of panel-to-panel connections at each vertical joint
n_h	Number of hold-downs on the uplift side of the shearwall
n_s	Number of angle brackets used along each panel
q	Gravity load
$\widetilde{q}$	Dimensionless load factor
r_f	Factored resistances of the panel-to-panel connections in shear
$r_{f,peak}$	Peak resistances of the panel-to-panel connections
$r_{f,peak,15}$	The 15th-percentile peak resistance of the panel-to-panel connections
r_h	Factored resistances of the hold-down in uplift
$r_{h,peak}$	Peak resistances of the hold-down.
$R_{s,r}$	Factored rocking resistance of CLT shearwalls under seismic loads
$R_{w,r,CP}$	Factored elastic strength of CLT shearwalls in CP behaviour
$R_{w,r,SW}$	Factored elastic strength of CLT shearwalls in SW behaviour
t_0	Total thickness of the longitudinal (vertical) CLT panel layers
t_{90}	Total thickness of the transverse (horizontal) CLT panel layers
t_{CLT}	Total thickness of the CLT panels
$t_{CLT,H}$	Total thickness of the CLT panels (vertical layers)
$t_{CLT,V}$	Total thickness of the CLT panels (horizontal layers)
t_{mean}	Mean thickness of the CLT panel layers
v_{35kN}	Deflection on the test envelope curve at a lateral load of 35 kN
$v_{F,\max}$	Displacement corresponding to the maximum force
v_u	Ultimate displacement
$v_{y,EEEP}$	Yield displacement as per the EEEP simulation
$v_{y,tri}$	Yield displacement as per the trilinear curve
$v_{y,EEEP}$	Yield displacement as per the EEEP simulation
$v_{y,tri}$	Yield displacement as per the trilinear curve
w	Width of the CLT boards
α	Parameter including the contribution of multiple angle bracket along the wall length
α_{CLT}	Parameter dependent on the lamella geometry of CLT wall panels
β	Ratio of one angle bracket's uplift stiffness to that of the hold-down
γ_{rh}	Over-strength factor ensuring yield hierarchy in CD
$\xi_{R,e}$	Panel-to-panel connection efficiency factor
Δ_q	Elastic lateral deflection of the CLT shearwall
Δ_w	Deflection due to the gravity load stabilizing impact
$\Delta_{w,F=35kN}$	Deflection at a lateral load of 35 kN

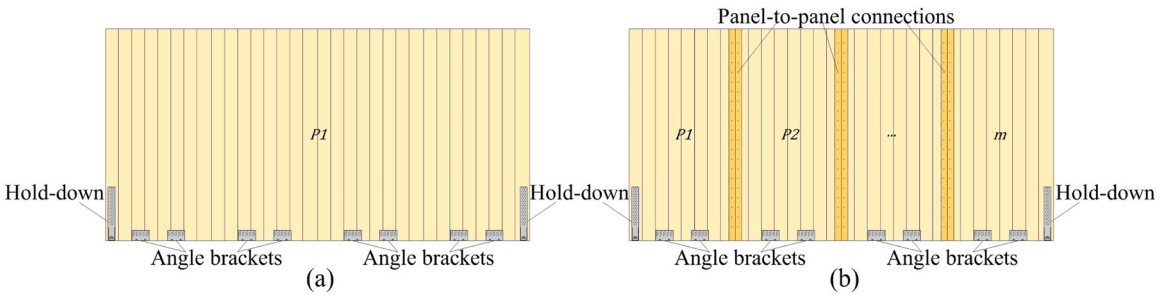


Fig. 1. CLT shearwall configurations: (a) single-panel; (b) multi-panel.

expected to generate more energy dissipative capability due to the use of relatively small diameter and slender connections like nails or screws.

Based on the mechanical properties of the connectors, three kinematic behaviours can be defined (Fig. 2): 1) Couple Panel (CP), where one point of rotation for each panel is attained, 2) Single Wall (SW), where only one global point of contact for the entire wall is attained, and 3) Intermediate (IN), which represents a special case, where only some panels are in contact with the ground.

Full-scale experimental tests have been conducted on complete CLT buildings subjected to lateral loads induced by simulated seismic forces [4–7]. It was consistently observed that building behaviour is dominated by the behaviour of the panel-to-panel connections and mechanical brackets used to anchor CLT shearwalls to the base (e.g., angle brackets and hold-downs). Moreover, the experimental results demonstrated a notable enhancement in the seismic performance of multi-panel CLT shearwalls compared to single-panel configurations. This improvement was attributed to the effective utilization of the ductility provided by the fasteners in the panel-to-panel connections.

Numerous research studies have been conducted on the lateral performance of isolated CLT shearwalls consisting of multiple panels [8–10, 3,11]. The outcome from these studies have also demonstrated that the panel-to-panel connections significantly contributed to the ductility and energy dissipation in the shearwalls. Although yielding initiated in the panel-to-panel connections, the ultimate failure was primarily observed in the mechanical anchors attaching walls to the base, such as hold-downs and angle brackets. This can be attributed to the use of hold-downs and angle brackets with comparatively lower resistance and stiffness in the abovementioned studies, which were primarily designed for light-frame timber shearwalls. Although an in-depth investigation of kinematic modes was not undertaken in previous studies, it was observed that the relative stiffness of hold-downs and panel-to-panel connections, along with the introduction of gravity loads, directly influenced the achieved kinematic modes. This encompassed the attainment of CP behaviour when employing relatively flexible panel-to-panel connections and, conversely, SW behaviour when utilizing relatively flexible hold-downs.

Ref. [12] conducted tests on two-panel CLT shearwalls subjected to cyclic loads using perforated-steel plates with self-drilling fasteners for both hold-down and panel-to-panel connections. CP behaviour was achieved, with the lateral behaviour and resistance primarily influenced by the panel-to-panel connections. Ref. [13] carried out experimental tests on three-panel CLT shearwalls subjected to monotonic lateral loads, employing relatively stiff shear key connections to attach the CLT panels together. The shearwalls displayed SW behaviour since the hold-down connections were more flexible compared to the panel-to-panel connections.

Several analytical approaches have been proposed to assess the behaviour of CLT shearwalls with different connection configurations. Refs. [9] and [14] proposed an analytical and an iterative displacement-based method, respectively, limited to single-panel and two-panel CLT shearwalls. These methods enabled the determination of lateral deflection, load capacity, and internal forces within connections. The contribution of hold-downs in light-frame timber and single-panel CLT shearwalls has been investigated, highlighting the importance of their deformation contribution [15]. A simplified capacity model for timber shearwall was introduced and validated against experimental tests with reasonable accuracy, and the corresponding over-strength factors were derived.

For multi-panel CLT shearwalls analytical expressions were developed to determine the kinematic modes and lateral load capacity and deflection, considering the elastoplastic properties of connections [16]. These analytical expressions were verified against numerical models, demonstrating their mathematical accuracy, with some limited validation against experimental tests involving two-panel CLT shearwalls. The deflection expressions to be used in the new generation of Eurocode 5 were investigated against numerical models involving single- and multi-panel CLT walls. The analytical expressions showed good agreement overall, with rocking exhibiting the greatest deviations and cases with gravity loads also showing greater discrepancies.

Capacity-based design (CD) methods for multi-panel CLT shearwalls have been introduced [17,18], considering cases without and with the uplift contribution of angle brackets, respectively. The primary aim was to ensure sufficient ductility and energy dissipation within the walls during seismic events. To achieve this, panel-to-panel connections were identified as the primary source of ductility, serving as the initial yielding elements. Subsequently, hold-down connections were designated as the secondary yielding elements, contributing further ductility to the system. Angle brackets were given a level of protection that ensures they remained elastic, avoiding the introduction of excessive sliding.

While the studies reviewed above focus primarily on single-storey shearwall configurations, extending multi-panel CLT shearwall behaviour to multi-storey systems introduces additional complexity through floor-wall interaction. Masroor et al. [19] conducted two-storey platform-type CLT shearwall tests and demonstrated that tension strap (TS) stiffness at the floor-wall interface significantly influences rocking behaviour. More flexible TS connections produced larger rocking displacements and greater inter-storey drift discrepancies between storeys, whereas matching the stiffness of the first-storey hold-down and second-storey TS connections promoted more uniform drift distribution.

D'Arenzo et al. [20,21] developed analytical framework that explicitly incorporates floor-wall interaction, demonstrating that this coupling can influence the lateral resistance, alter deflection profile, and generate kinematic modes that deviate from single-storey predictions. Masroor et al. [22] further extended this work to multi-panel walls, deriving matrix-form expressions for elastic lateral deflection that incorporate floor-wall and wall-to-floor connection behaviour; comparisons with CSA O86–24 [1] revealed that floor-wall interaction provides additional restraint that meaningfully reduces lateral deflection, which is not captured by current design provisions. Mallardi et al. [23] investigated platform-type multi-storey CLT shearwalls with perpendicular walls, identifying the influence of orthogonal wall connections on the lateral response and providing analytical and numerical frameworks for their assessment.

The single-storey results developed in this study is expected to provide the mechanistic basis needed to extend CLT shear-wall design to multi-storey systems, because they isolate the two fundamental kinematic modes (CP and SW) and quantify how relative stiffness between panel-to-panel joints and hold-downs governs mode selection, deformation compatibility, and connection demand. These stiffness

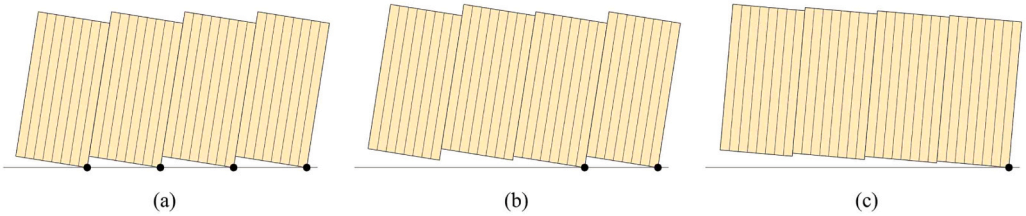


Fig. 2. CLT shearwall kinematic modes: (a) CP; (b) IN; (c) SW.

hierarchies directly translate to multi-storey behaviour once floor-wall coupling, diaphragm continuity, and orthogonal wall restraint are introduced, since stiffer floor systems and stronger inter-storey connections tend to suppress differential panel rotation and promote SW-type response, whereas more flexible floor interfaces allow CP-type mechanisms to persist across levels. By establishing validated per-storey parameters, yielding sequences, and stiffness ratios, the present single-storey characterization provides the essential inputs required by existing multi-storey analytical frameworks and forms a rigorous foundation for modelling and developing design provisions that accurately capture the lateral response of multi-storey platform-type CLT buildings.

In light of the current state of knowledge, this research study aims to address several key objectives related to single-storey, multi-panel CLT shearwalls. The primary goal is to quantify the kinematic modes as a function of the relative stiffness of connections, which is an aspect that has received limited attention in earlier research concerning multi-panel configurations. Furthermore, the behaviour of connections and their contribution to the lateral load resistance, ductility, and failure modes are studied. This includes systematic investigations of connection yielding and failure hierarchies, particularly within the context of established capacity-based design approaches for CLT shearwalls aimed at achieving specific levels of ductility and energy dissipation.

Another significant novelty in this research is the investigation of shearwalls comprised of more than two panels, and the effects of additional dead loads. The research study also deviates from previous studies in utilizing the latest generation of connections consisting of high-capacity hold-downs and angle brackets.

Comparisons between numerical models and experimental tests were conducted to demonstrate the applicability of a simplified finite element model, in which the connections are represented by envelope curves derived from corresponding connection-level tests, in predicting the kinematic mode and the elastic and plastic behaviour of the walls. The design expressions provided in the 2024 edition of CSA O86-24 [1] are also evaluated by comparison with test results to assess their effectiveness in predicting elastic strength, deflection, plastic strength, and kinematic mode. This comparison contributes to the validations of these recently introduced design expressions against experimental results involving different geometries, connection layouts, and gravity loads.

2. Materials and methods

The focus of this paper is on two configurations, namely CLT shearwalls where sliding is prevented in order to investigate the contribution of conventional hold-down and panel-to-panel connections alone, and CLT shearwalls with angle brackets positioned along the wall length in order to investigate their additional contribution in resisting sliding and uplift. The primary focus of this study is on single storey shearwalls, providing fundamental insight into the underlying kinematic modes and connection behaviour, and establishing a basis for future extensions to multi-storey multi-panel applications.

2.1. Materials

The experimental tests utilized E1 stress grade CLT panels manufactured in accordance with ANSI/APA (2020) [24] and composed of three layers, each board with a thickness of 35 mm and width of 89 mm, resulting in a total thickness of 105 mm. This configuration is representative of commercially available products used for platform-type CLT shearwalls in low- to mid-rise construction, and its thickness and mechanical properties are consistent with current design practice. Throughout the tests, the CLT panels were kept under controlled climate conditions, maintaining a temperature of 20 ± 2°C and a relative humidity of 65 ± 5%. Consequently, the moisture content of the panels remained at 10 ± 2%.

Fig. 3 outlines the connections used in the shearwalls. For hold-down connection (Fig. 3-a), WHT620 [25] was employed at the ends of the

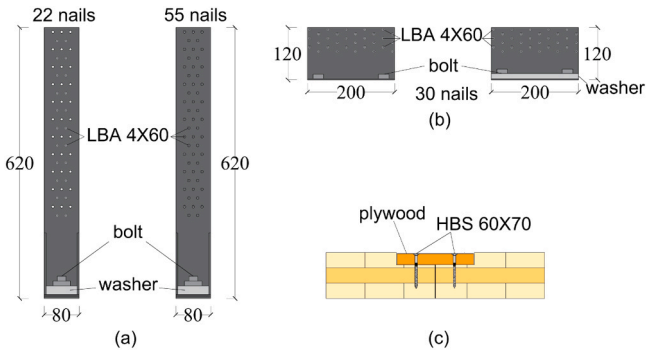


Fig. 3. (a) WHT620 hold-down (b) TCN200 angle bracket (c) splined joint panel-to-panel connection.

walls. To investigate different uplift resistance and stiffness, two nailing patterns were utilized: fully nailed (fifty-five 4 ×60 annular ring shank nails) and partially nailed (twenty 4 ×60 annular ring shank nails). The angle brackets (Fig. 3-b) consisted of TCN200 [26] with fully nailed pattern comprising thirty 4 × 60 annular ring shank nails, and in most cases, no washer was employed. Another combination that was tested included replacing the hold-down with fully nailed angle brackets with washer. The CLT panels were connected together using a spline joint (Fig. 3-c) with 1" (25.4 mm) thick Douglas-Fir Plywood (DFP), fastened with HBS 6 × 70 self-tapping screws (STS) [27].

2.2. Test configurations and set-up

Table 1 presents the details of the twelve shearwall specimens investigated in this study. Among these, five walls (i.e., walls #1-#5) were tested without angle brackets ($n_s = 0$), but where sliding was prevented (Series A), while the seven remaining walls (i.e., walls #6-#12) included angle brackets to resist sliding ($n_s \neq 0$) (Series B). n_s represents the number of angle brackets used along each panel. The former configuration was meant to intentionally eliminate the contribution of the angle brackets and to simplify the analysis, while the latter represents a more realistic shearwall performance. For five test configurations, a gravity load, q, equivalent to a uniformly distributed load of 5.22 kN/m, was applied to the top face of each panel. Variables b and h represent the length and height of each panel, respectively, m represents the number of panels, while B denotes the total length of the wall ($b \bullet m$). Additionally, n_h indicates the number of hold-downs on the uplift side of the shearwall and n_f signifies the number of panel-to-panel connections at each vertical joint. The selected configurations were chosen based on preliminary numerical models in order to achieve distinct kinematic modes. More details on the proposed numerical model are provided in Section 4.

Fig. 4 displays the wall configurations, showcasing the panel sizes and connections employed. Walls #1 to #5 featured a cut at the bottom corner of the panels where rotation occurs, allowing for the installation of supports to prevent sliding since no angle brackets were utilized. Walls #6, #7, and #9 to #12 consisted of fully nailed angle brackets without washers, along with hold-downs. In wall #8, the hold-down was substituted with fully nailed angle brackets with washer.

Fig. 5 illustrates the test set-up for walls without angle brackets (walls #1 to #5). To transfer the horizontal load, each panel was equipped with a steel plate attached at the top and center of the panel using twenty-six HBS 6× 70 mm. Additionally, an E-shaped steel plate was affixed to the actuator and two steel channels, C5@9, with a length of 4060 mm. A fitted connection was employed to connect the top steel plates on each panel to the two channels in order to ensure equal displacement across all panels. This mechanism simulated diaphragm behaviour at the top of the wall. These connections were secured by using steel nuts of the same size as the holes in the steel plates and

Table 1
Shearwall-level tests information.

Wall Series	Wall ID	q (KN/m)	$b \times h$ (m)	B (m)	n_h	m	n_s	n_f	Expected mode
A	#1	0	1.22 × 2.44	3.66	2	3	0	9	CP
	#2	5.22	1.22 × 2.44	3.66	2	3	0	9	CP
	#3	0	1.22 × 2.44	3.66	1	3	0	35	SW
	#4	5.22	1.22 × 2.44	3.66	1	3	0	35	SW
	#5	5.22	1.22 × 2.44	3.66	1	3	0	26	SW
B	#6	0	1.22 × 2.44	3.66	2	3	2	9	CP
	#7	5.22	1.22 × 2.44	3.66	2	3	2	9	CP
	#8	0	1.22 × 2.44	3.66	2	3	2	9	CP
	#9	0	1.22 × 2.44	3.66	1	3	2	35	SW
	#10	5.22	1.22 × 2.44	3.66	1	3	2	35	SW
	#11	0	1.22 × 2.44	2.44	2	2	2	9	CP
	#12	0	0.61 × 2.44	2.44	2	4	1	9	CP

channels, connected together with threaded rods. Lateral supports were provided at two points on each face of the test shearwalls, using the support system shown in Fig. 6, consisting of steel I-section columns and hollow section beams placed at each face of the wall to avoid out of plane lateral displacement or buckling. Fig. 7 illustrates the gravity load system in CLT shearwall tests, where two concrete blocks with a total mass of 600 kg were hung from each side of the panels. It is noteworthy to mention that the gravity load was applied as a real dead load without imposing any restraint on the panels. Table 2 summarizes the details of each connection.

A hydraulic actuator, with a maximum compression capacity of 365 kN, was used to transfer the lateral load to the shearwall specimen. A displacement rate of 6 mm/min was selected in order to maintain consistency with the displacement rates employed in connection tests described in Masroor [29].

Nine cable transducers were utilized to measure the various wall displacements, as shown in Fig. 5.

Table 3 presents the position and direction of each channel. v.1 was used to measure the vertical displacement in the first panel, representing the uplift in the hold-down. v.2 and v.3 were used to measure the vertical displacement at the point of rotation of the first and second panel, respectively, indicating whether these panels maintain contact with the ground. sh.1 and sh.2 were used to measure the vertical displacement at the point of rotation of the first panel relative to the uplift side of the second panel and the vertical displacement at the point of rotation of the second panel relative to the uplift side of the third panel, respectively. s.1 and s.2 measured the horizontal (sliding) displacements at the bottom of the first and third panels, respectively, while t.1 and t.2 measured the respective horizontal displacements of the first and third panels at their top. Channel F represents the horizontal load of the actuator.

3. Results and discussion

The experimental envelope curves, lateral load versus wall top displacement, as well as the results obtained from numerical models (presented in detail in Section 4) are illustrated in Fig. 8. Furthermore, Table 4 and Table 5 present a comprehensive summary of the mechanical properties obtained from the shearwall tests, including maximum force, corresponding displacement, ultimate displacement, properties derived from Equivalent Energy Elastic Plastic (EEEP), based on Ref. [28], and tri-linear curves, based on Ref. [29].

It can be noted that the general shape of the curves along with the summarized mechanical properties with and without gravity loads appear to be similar for the same configurations (e.g., comparisons of wall #1 versus #2 and wall #3 versus #4); however, adding gravity load is observed to have resulted in greater maximum resistances while its impact on other properties such as stiffness and ductility appeared to be relatively insignificant.

It can also be observed that walls with SW behaviour (i.e., walls #3-#5, and #9-#10) had greater stiffness, nearly double, but lower ultimate displacement and ductility than walls with CP behaviour. This can be attributed to the number of panel-to-panel connections involved in the deformation mechanism of the wall exhibiting CP behaviour. Wall #5, which involved fewer panel-to-panel connections compared to walls #3 and #4, exhibited more flexible and ductile behaviour.

The ductility ratios ranged from 2.0 to 2.9 in CP behaviour and from approximately 1.7–2.3 in SW behaviour. Despite involving different yielding sequence and failure mechanisms, the two kinematic modes produced comparable ductility ratios. In CP behaviour, hold-downs reached their ultimate displacement relatively soon after yielding, limiting the available post-yield displacement and constraining the global ductility. In SW behaviour, although the hold-downs also governed the response, panel-to-panel connections, whose yield displacement is approximately half that of hold-downs [29], remained partially engaged throughout loading, providing residual flexibility that partially compensated for the more limited deformation capacity of the hold-down. Moreover, walls with CP behaviour exhibited significantly greater ultimate displacement, ranging from 58 to 70 mm, compared to walls with SW behaviour, which had ultimate displacements of approximately 21–41 mm. Notably, for wall #8, where hold-downs were replaced with angle brackets with washers, a higher ductility ratio of over 3.3 was achieved.

The reported ductility ratios indicate that, in CP behaviour, the full deformation capacity of panel-to-panel connections is not entirely exploited, as hold-down reached their ultimate deformation and failed prior to the panel-to-panel connections reaching their potential deformation capacity. This observation is directly relevant to the development and refinement of capacity-based seismic design approaches for seismic applications, as it highlights the need to ensure that hold-downs possess sufficient deformation capacity to avoid prematurely limiting system-level ductility. Connection-level cyclic tests reported in Ref. [29] indicated limited low-cycle fatigue effects for the connection types used in this study, suggesting that the ductility values reported here are broadly representative of those expected under seismic loading conditions.

Walls incorporating angle brackets demonstrated notably higher resistance. For example, in CP behaviour, wall #6 exhibited a resistance of approximately 164 kN, whereas the same configuration without angle brackets (wall #1) only had a resistance of approximately 130 kN. This represents an approximate 26% increase in resistance, emphasizing the significant contribution of angle brackets to the rocking and lateral behaviour of CLT shearwalls. Similarly, in SW behaviour, the difference in resistance between walls #3and #9 was approximately 37%, further underscoring the substantial influence of angle brackets in this kinematic mode. These findings are consistent with the sensitivity analyses presented in Masroor et al. [16], wherein the contribution of angle brackets to the rocking behaviour appeared to be more prominent for SW than CP behaviour.

Comparing the use of four narrow CLT panels (wall #12) to the same total length wall with two panels (wall #11), it is evident that the former

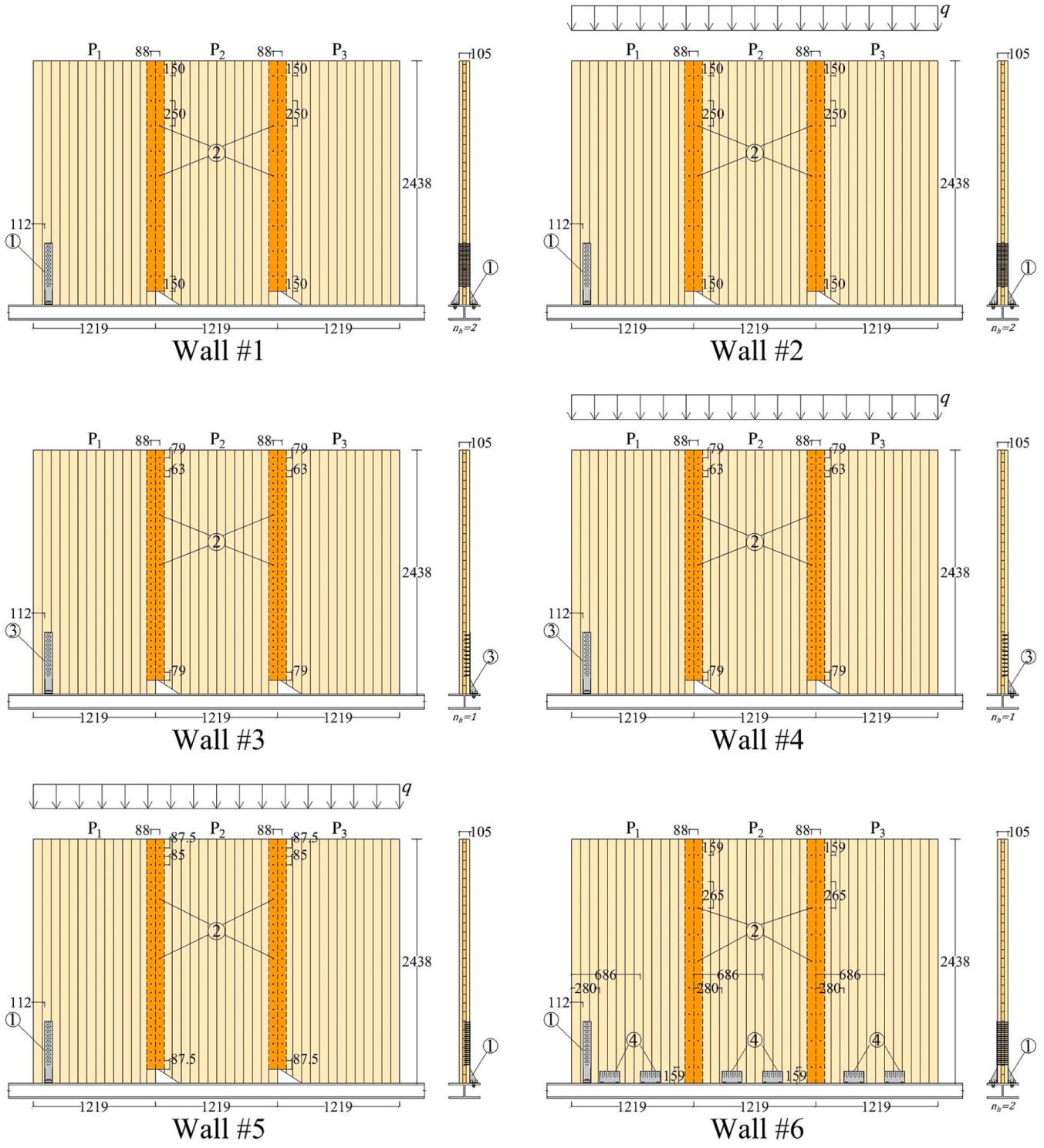


Fig. 4. Shearwall configurations.

had significantly lower resistance, around 76 kN, compared to the latter, which had a resistance of around 120 kN. Wall #11 also displayed more than triple the stiffness obtained in wall #12. This increase in aspect ratio led to a significant reduction in lateral resistance, while only minor improvement was improved in ductility.

3.1. Kinematic modes

The kinematic modes observed from the full-scale shearwall tests were consistent with those predicted based on the preliminary numerical models (see also Table 1). For walls #1, #2, #6-#8, and #11-#12 CP mode was achieved (Fig. 9-a), while SW mode was attained for walls #3-#5 and #9-#10 (Fig. 9-b). Fig. 10 illustrates the uplift displacement of the three panels at their rotation points. The figure also includes two sets

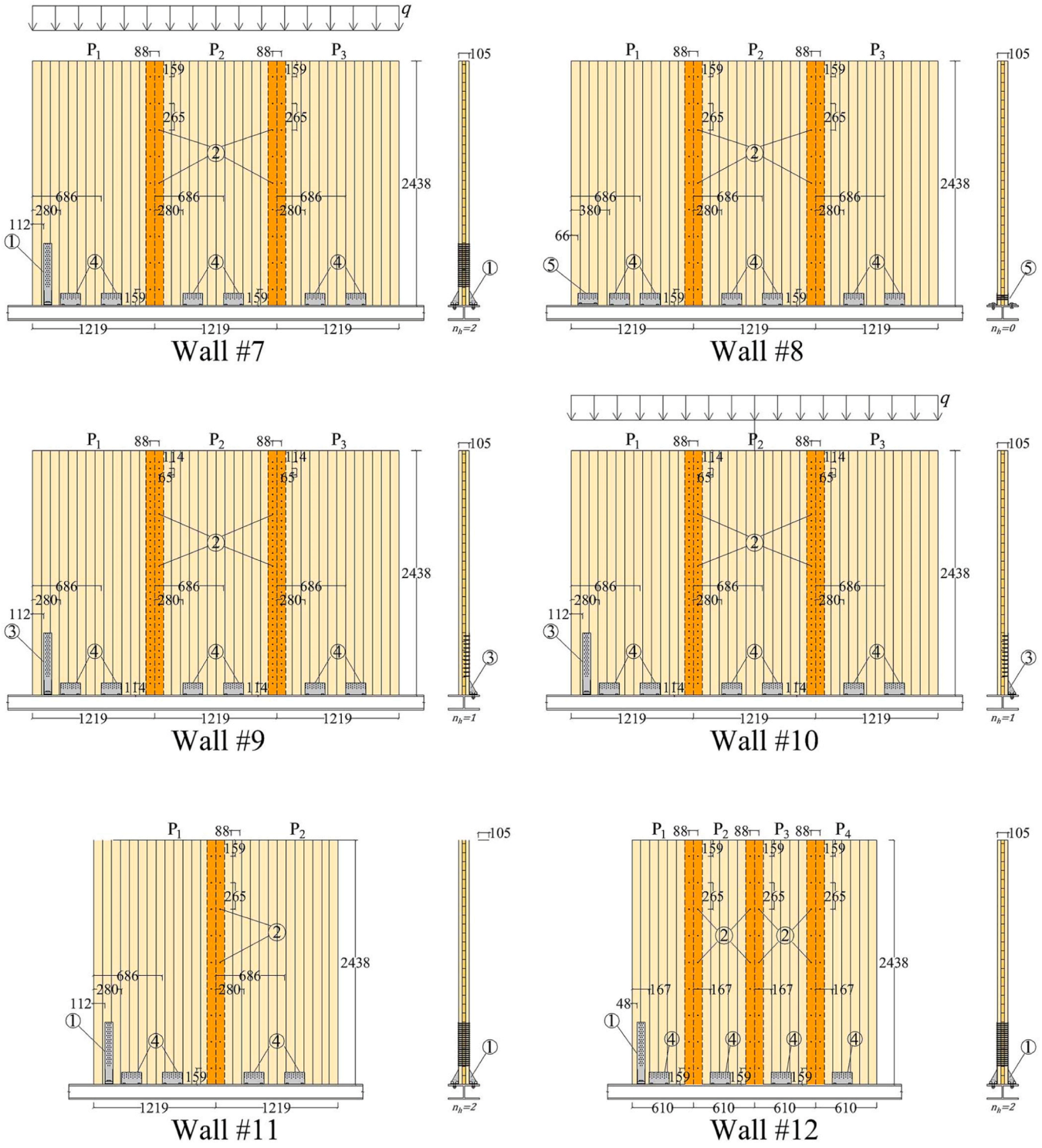


Fig. 4. (*continued*).

of examples for walls with sliding prevention supports and those with angle brackets exhibiting CP and SW behaviours, serving as illustrative examples.

The observed behaviour was also consistent with the assumption about the activation load, where for example for all walls with SW behaviour, the panels initially remained in contact with the ground until the stabilizing effect of gravity load was overcome, and the entire wall rotated.

3.2. Yield hierarchy

Fig. 11 illustrates two sets of curves depicting the total top lateral displacement as a function of the uplift displacement and slip between panels. Two examples of walls exhibiting CP and SW behaviour are depicted for each configuration with and without angle brackets. Additionally, two horizontal lines are plotted, associated with the average yield displacements of the hold-downs and panel-to-panel connections, based on the results obtained from connection-level tests presented in (Masroor [29]).

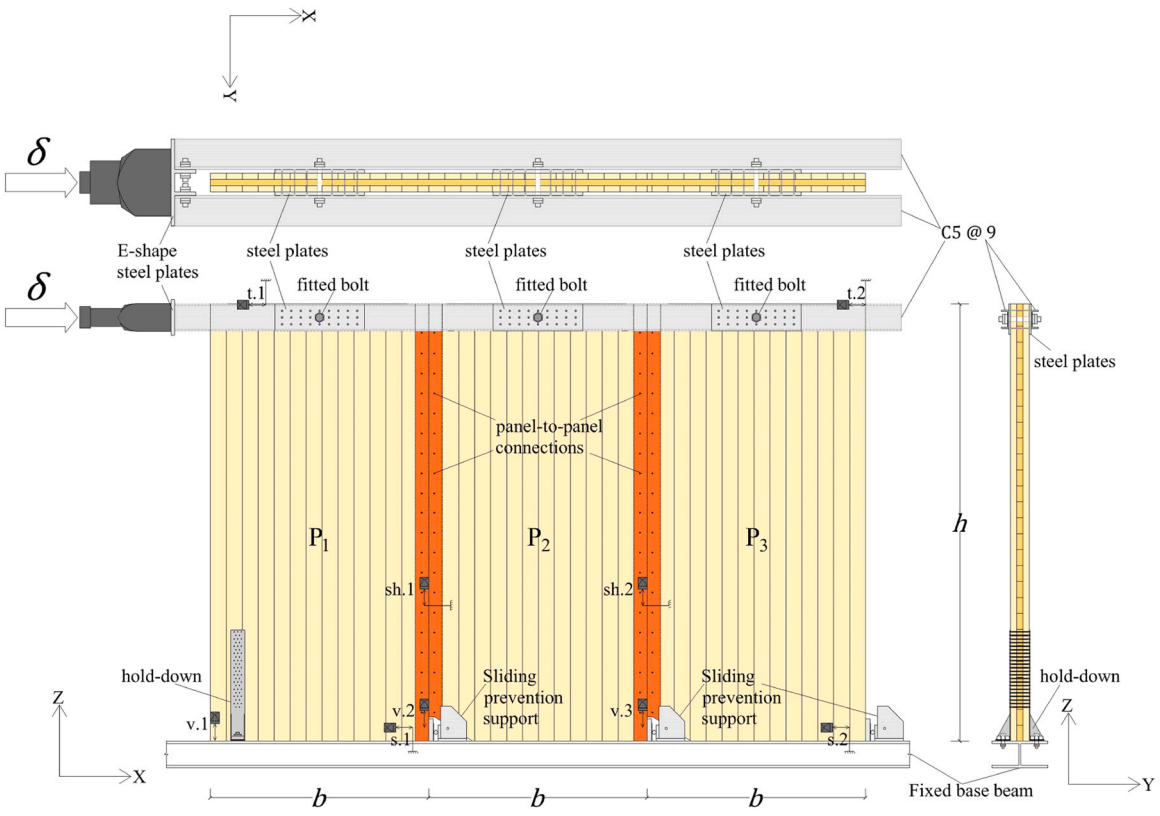


Fig. 5. Schematic Set-up of CLT shearwall-level tests.

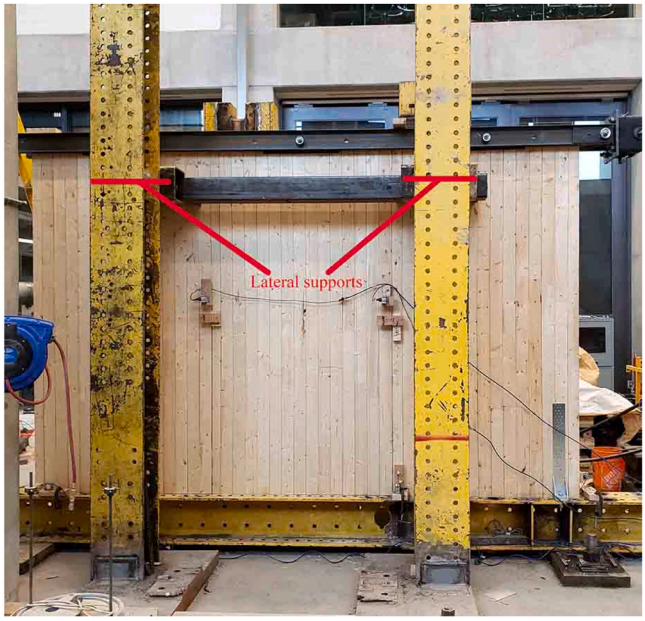


Fig. 6. Lateral support used in experimental tests.

The curves for walls with CP behaviour, shown in Fig. 11-a and Fig. 11-c, exhibited reasonably similar patterns of uplift and slip, which is consistent with what is anticipated in CP behaviour. This observation confirms that equal displacements were effectively transferred to each panel, resulting in consistent rotations across all panels. As expected, the uplift displacement, v.1, was higher than the relative slips for walls with SW behaviour, sh.1 and sh.2, shown in walls #3 and #9, since relatively stiff panel-to-panel connections were used.

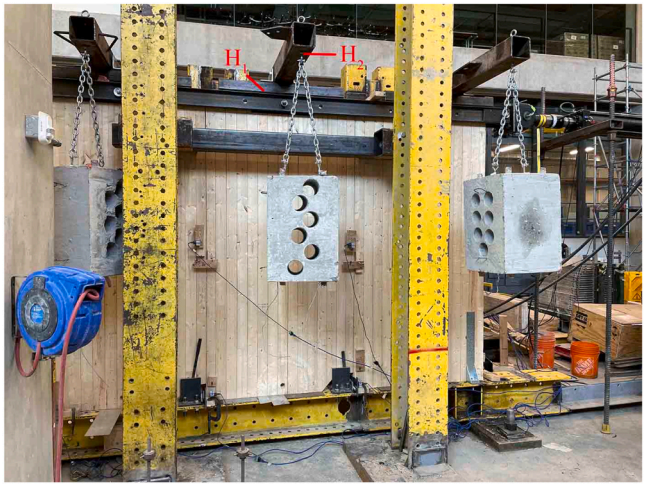


Fig. 7. Supplementary gravity loads.

The experiments showed distinct yielding sequences among panel-to-panel connections and hold-downs for walls with CP mode and SW mode. In CP mode, panel-to-panel connections yielded before the hold-downs, while in SW mode walls, the panel-to-panel connections remained elastic throughout the tests, and the hold-down yielded and failed. This observation is consistent with the yield hierarchy criteria put forth by Casagrande et al. [17] and Masroor et al. [18], with panel-to-panel connections yielding initially, followed by hold-downs to fulfill the capacity-based design requirement.

In the case of wall #5 with SW mode, the hold-down began yielding before the panel-to-panel connections, and subsequently, the panel-to-panel connections yielded before the ultimate failure of the hold-down.

Table 2
Connections used in shearwall-level tests.

Connection ID	Specification
(1)	• Hold-down WHT620 • 1 bolt | M20 × 100 mm • 1 washer 70 × 77 × 20*mm* | WHTW70 • 55 nails | LBA 4 × 60 mm
(2)	• Panel-to-panel connection • Screw HBS 6 × 70 mm
(3)	• Hold-down WHT620 • 1 bolt | M20 × 100 mm • 1 washer 70 × 77 × 20*mm* | WHTW70 • 22 nails | LBA 4 × 60 mm
(4)	• Angle bracket | TCN200 • 2 bolts | M12 × 60 mm • 30 nails | LBA 6 × 40 mm
(5)	• Angle bracket | TCN200 • 2 bolts | M12 × 60 mm • 1 washer 190 × 72 × 12*mm* | TCW200 • 30 nails | LBA 6 × 40 mm

Table 3
Measurement channels.

Parameter	Position	Direction
v.1	Uplift side of the first panel	Vertical (uplift)
v.2	Point of rotation of the first panel	Vertical (uplift)
v.3	Point of rotation of the second panel	Vertical (uplift)
sh.1	Panel 1 and panel 2	Relative vertical (shear)
sh.2	Panel 2 and panel 3	Relative vertical (shear)
s.1	Bottom of panel 1	Horizontal (sliding)
s.2	Bottom of panel 3	Horizontal (sliding)
t.1	Top of panel 1	Horizontal
t.2	Top of panel 3	Horizontal
F	Actuator	Horizontal (load)

3.3. Failure modes

Fig. 12 illustrated the behaviour of the connections before and after their failure. The ultimate failure mechanisms consistently occurred in hold-down connections, which can be attributed to the lower ultimate displacement of hold-downs compared to the panel-to-panel connections. It was observed that walls with fully nailed hold-downs (i.e., walls #1, #2, #5, #6, #7, #11, and #12) experienced uplift failure, consisting of tensile failure in the vertical steel plate near the first row of nails, as shown in Fig. 12 (a). The walls with partially nailed hold-downs (i.e., walls #3, #4, #9, and #10) also exhibited uplift failures, but where the nail fasteners failed due to the head breakage combined with nail withdrawal and bending, as shown in Fig. 12 (b). For wall #8, as hold-downs were replaced with fully nailed angle brackets, failure occurred in the end angle brackets due to the bolts' breakage, as shown in Fig. 12 (c).

4. Numerical models: validation

This section provides a comparison between the finite element modelling conducted using the SAP2000 package [31] and the experimental results, in order to illustrate the applicability of modelling techniques widely used in practice, with connections modelled using real load-deformation curves obtained from connection-level tests. Fig. 13 illustrates the numerical model configuration used, where the CLT panels were modelled as shell elements of size 61 × 61 mm, based on mesh sensitivity analysis presented in Ref. [30] The CLT panels were defined with orthotropic material properties. The required properties were obtained from Ref. [24] for E1 CLT grade, including E_0, E_{90}, and G_0, and were equal to 11700, 300, and 731 MPa, respectively. The effective moduli, utilized to define orthotropic material properties, $E_{eff,1}$ (along the horizontal direction), $E_{eff,2}$ (along the vertical direction), and G_{eff}, are obtained using Eqs. (1)-(4), based on work by Ref. [32], where α_{CLT} is a parameter derived from the lamella geometry of CLT wall panels and can be calculated using Eq. (3).

$$E_{eff,1} = \frac{E_0 \bullet t_{90} + E_{90} \bullet t_0}{t_{CLT}} = 4100 \quad MPa \tag{1}$$

$$E_{eff,2} = \frac{E_0 \bullet t_0 + E_{90} \bullet t_{90}}{t_{CLT}} = 7900 \quad MPa \tag{2}$$

$$\alpha_{CLT} = 0.53 \bullet \left(\frac{t_{mean}}{w}\right)^{-0.79} = 0.53 \bullet \left(\frac{35}{89}\right)^{-0.79} = 1.11 \tag{3}$$

$$G_{eff} = \frac{G_0}{1 + 6 \bullet \alpha \bullet \left(\frac{t_{mean}}{w}\right)^2} = 361.1 \quad MPa \tag{4}$$

Where t_0 and t_{90} are the total thicknesses of the longitudinal (vertical) and transverse (horizontal) layers, equal to 70 and 35 mm, respectively, t_{CLT} is the total thickness of the panel and is equal to 105 mm for three-layer panels, t_{mean} is the mean thickness of the CLT panel layers (35 mm), and w is the width of the boards, equal to 89 mm.

The connections in the model were represented using multi-linear link elements, which were based on envelope curves derived from connection-level experimental tests. Mechanical anchors, such as hold-downs, were assumed to be active only in uplift due to their minimal contribution to shear, whereas angle brackets were considered for both uplift and shear. To simulate the contact bearing between the CLT panels and the foundation or floor below, rigid gap elements were employed with zero tension stiffness and compression properties.

A vertical gravity load was uniformly applied on top of each panel. For all walls, an additional 1.45 kN/mm was included to account for the self-weight of the CLT panels, resulting in total gravity loads of 1.45 and 6.67 kN/mm for walls without and with superimposed gravity loads, respectively. A concentrated lateral load was applied to the left corner, 75 mm below the top of the CLT walls, which aligns with the loading actuator position used in the experimental tests. Diaphragm constraints were applied at the top and bottom of the panels, consistent with the assumptions made in the experimental tests.

Fig. 14 illustrates the average load-displacement envelope curves, obtained from Ref. [29], of fully- and partially nailed WHT620 hold-downs under uplift loading and HBS 6 × 70 mm fasteners used as panel-to-panel connections under shear loading, respectively. In order to facilitate the incorporation of the interaction between shear and uplift based on the circular domain for bi-directional angle brackets, it was necessary to utilize elastic-perfectly-plastic simulations as shown in Fig. 15 [29]. The mechanical properties of angle brackets with washers under shear were considered equal to those without washers since the behaviour and failure were dominated by the nails. The interaction between shear and uplift for angle brackets was simulated through a macro element representing the circular domain [33].

The load-displacement curves obtained from experimental tests and those derived from numerical models were presented in Fig. 8. It can be observed that the numerical models showed a reasonable match for all walls. Both CP and SW behaviour exhibited reasonable accuracy in terms of the elastic stiffness. The numerical models appropriately predicted the plastic regions, capturing yielding and local failure in the connections. SW behaviour showed a better match compared to CP, particularly in the plastic region. This can be attributed to the fact that the panel-to-panel connections remained elastic, while only the nonlinearity from hold-downs and angle brackets were incorporated. This resulted in less complex models for SW walls and, consequently, reduced discrepancies between numerical and experimental tests.

Regarding kinematic modes, consistent behaviours were observed between the experimental and numerical results. Furthermore, the yield hierarchies established for CP and SW behaviour were consistent with the previously presented experimental results.

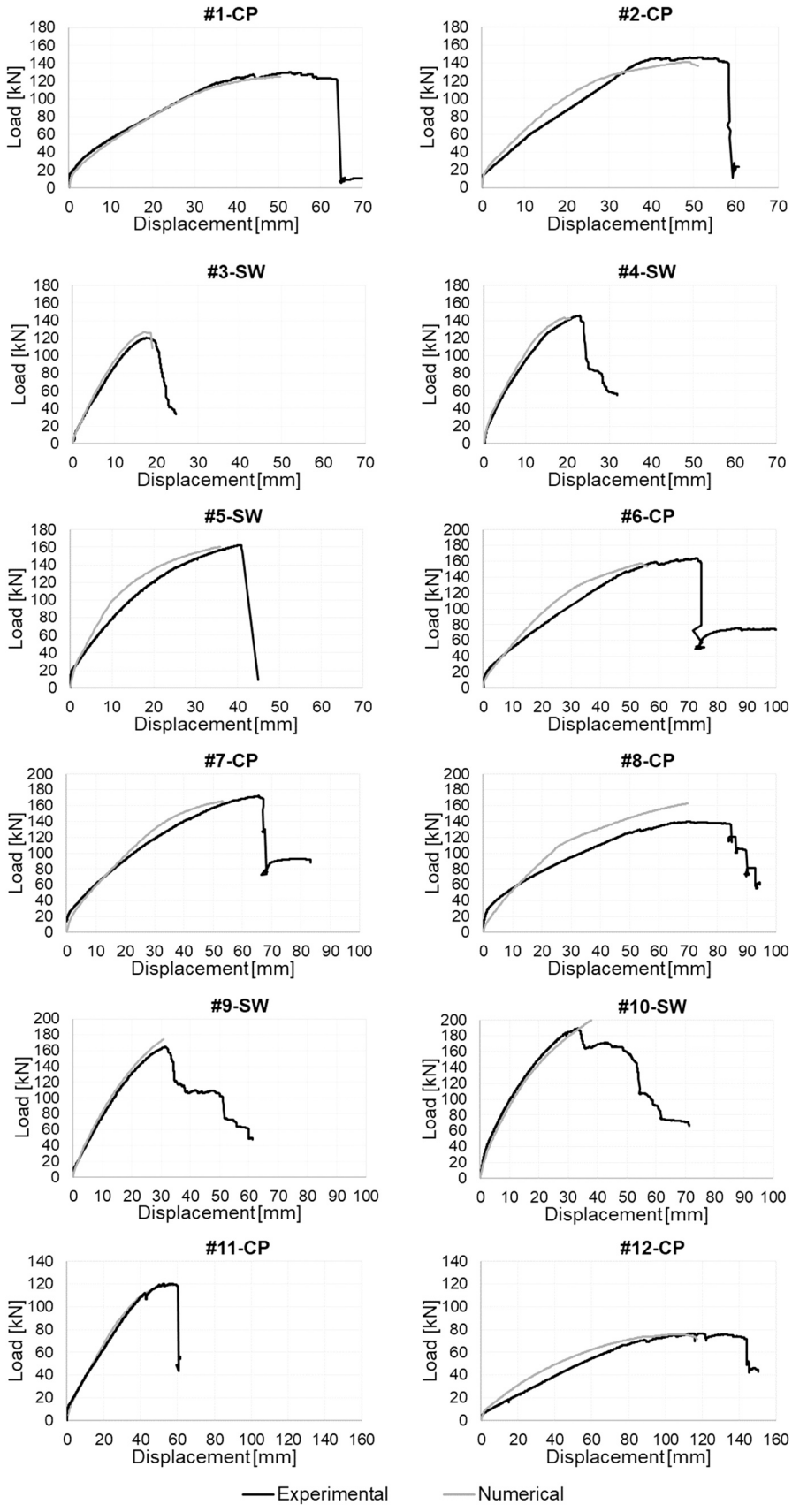


Fig. 8. Lateral load vs the top displacement.

Table 4
Mechanical properties of shearwall-level tests without angle brackets, Series A.

Parameter	Unit	CP		SW		
		#1	#2	#3	#4	#5
F_{max}	[kN]	130.1	146.4	120.2	145.3	162.3
$v_{F,max}$	[mm]	53.0	49.3	17.7	23.0	40.7
v_u	[kN]	64.1	58.3	20.8	24.1	41.1
$F_{y,EEEP}$	[mm]	115.5	134.3	109.5	126.0	140.7
$v_{y,EEEP}$	[mm]	23.4	29.4	11.8	11.6	19.0
$k_{e,EEEP}$	[kN/mm]	4.9	4.6	9.3	10.8	7.4
$D_{m,EEEP}$	[-]	2.7	2.0	1.8	2.1	2.2
$F_{y,tri}$	[kN]	109.9	136.1	111.3	127.5	139.2
$v_{y,tri}$	[mm]	22.1	29.8	12.0	11.8	18.8
$k_{e,tri}$	[kN/mm]	5.0	4.6	9.3	10.8	7.4
$D_{m,tri}$	[-]	2.9	1.9	1.7	2.0	2.2

Table 6 summarizes the key parameters obtained from each method, including the percentage difference between experimental test and numerical model results denoted as $\xi_{T/N}$. The last three rows indicate the maximum, minimum, and mean values of $\xi_{T/N}$. The results showed that the maximum and yield forces, $F_{\max}$ and $F_{y,EEEP}$, respectively, matched reasonably well with a difference in the range of 0.4%−15.1%. The associated displacements with the maximum and yield forces, $v_{F_{\max}}$ and $v_{y,EEEP}$, respectively, showed slightly higher discrepancies with mean differences of 8.7% and 17.3%, respectively. As for the elastic stiffness, $k_{e,EEEP}$, the differences were in the range of 1.0–20.3%, except for wall #5 where the difference was 33.7%. As seen in Fig. 8, the numerical and experimental curves remain in close agreement in terms of overall shape, peak load, and displacement capacity, with the deviation confined to the initial stiffness branch. This is consistent with the well-known difficulty of capturing initial stiffness in timber tests, where connection seating, initial slip, and material variability introduce additional flexibility that is not represented in idealized numerical models. A discrepancy of 4.7%−29.3% was observed in the ultimate displacement, v_u, with the upper bound reflecting cases where the numerical model, which employs idealized envelope curves with a fixed failure displacement criterion, could not fully capture the experimentally observed post-peak degradation and failure mechanism. It is noteworthy to mention that the deviations between the numerical and experimental results can be attributed to the inherent variability of the wood material and connection behaviour, as well as modelling simplifications, such as neglecting friction between the panels and the base and loading fixtures, as well as adopting idealized connection behaviour (e.g., ignoring the contribution of hold-downs in horizontal shear).

5. Comparison with existing analytical models

This section compares experimental results with the analytical expressions found in the 2024 edition of CSA O86–24 [1] to evaluate their ability to predict the lateral performance of single-storey multi-panel CLT shearwalls. The assessment covers comparison between: (1) analytical elastic resistance and the yield load from the trilinear curves obtained from the experimental tests; (2) elastic displacement at the lateral load of 35 kN and the corresponding displacement on the experimental envelop curves; (3) predicted CP and SW kinematic modes and those observed in tests; (4) yield hierarchy from the capacity-based design and that achieved in tests; (5) analytical plastic resistance and the maximum load from the envelope curves for those shearwalls where hierarchy of yielding between vertical joints and hold-down is achieved. It should be noted that walls without uplift contribution from angle brackets (Series A) are developed for both CP and SW elastic behaviour, whereas walls with uplift contribution from angle brackets (Series B) are

Table 5
Mechanical properties of shearwall-level tests with angle brackets, Series B.

Parameter	Unit	CP			SW		CP	
		#6	#7	#8	#9	#10	#11	#12
F_{max}	[kN]	164.0	172.3	140.1	164.6	189.5	120.1	76.5
$v_{F,max}$	[mm]	73.1	65.7	70.8	31.5	33.6	55.5	118.0
v_u	[kN]	74.4	67.6	84.9	34.5	36.0	60.2	144.9
$F_{y,EEEP}$	[mm]	146.1	147.4	120.5	145.4	161.7	112.1	71.9
$v_{y,EEEP}$	[mm]	38.6	31.1	25.4	19.6	15.5	37.2	78.6
$k_{e,EEEP}$	[kN/mm]	3.8	4.8	4.8	7.4	10.4	3.0	0.9
$D_{m,EEEP}$	[-]	1.9	2.2	3.3	1.8	2.3	1.6	1.8
$F_{y,tri}$	[kN]	146.7	147.7	106.7	150.4	161.3	111.8	70.5
$v_{y,tri}$	[mm]	38.7	31.1	22.1	20.3	15.5	37.1	76.9
$k_{e,tri}$	[kN/mm]	3.8	4.7	4.8	7.4	10.4	3.0	0.9
$D_{m,tri}$	[-]	1.9	2.2	3.8	1.7	2.3	1.6	1.9

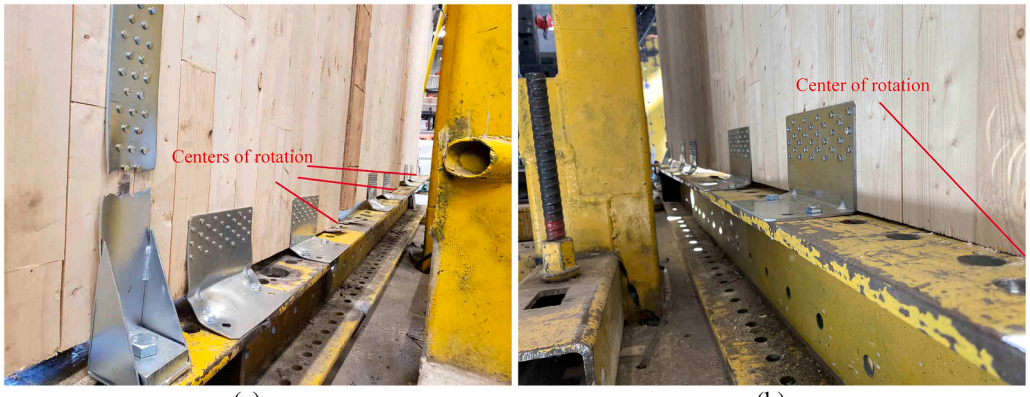


Fig. 9. Examples of kinematic mode after failure for shearwall tests: (a) CP and (b) SW.

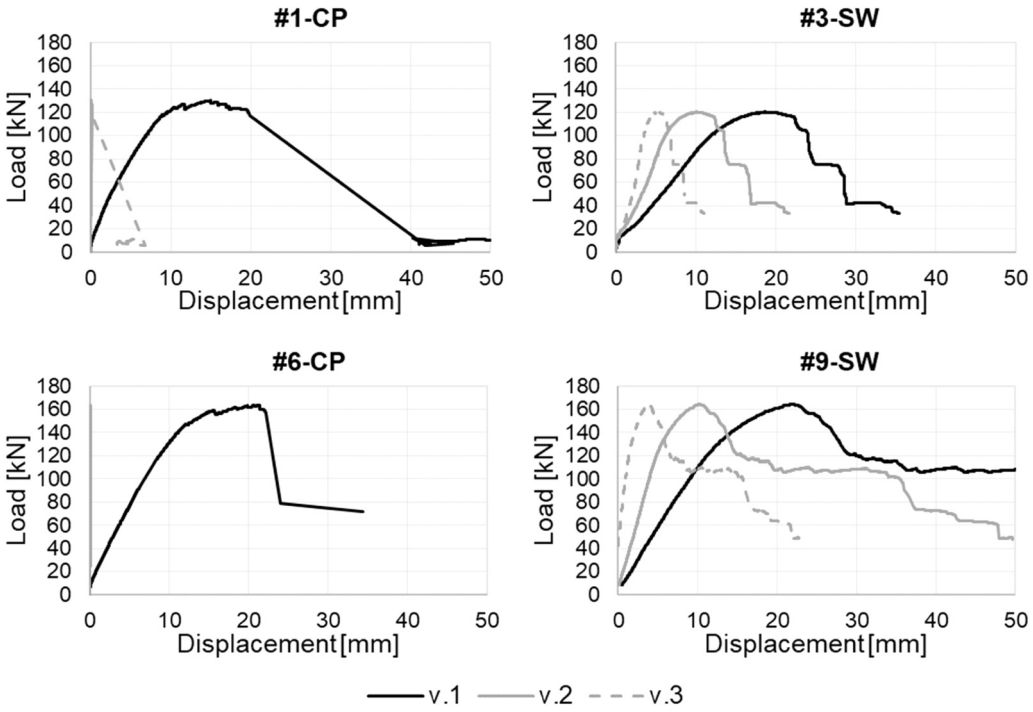


Fig. 10. Lateral load vs uplift of the first panel (v.1) and uplift of rotation of the first and second panels (v.2, & v.3).

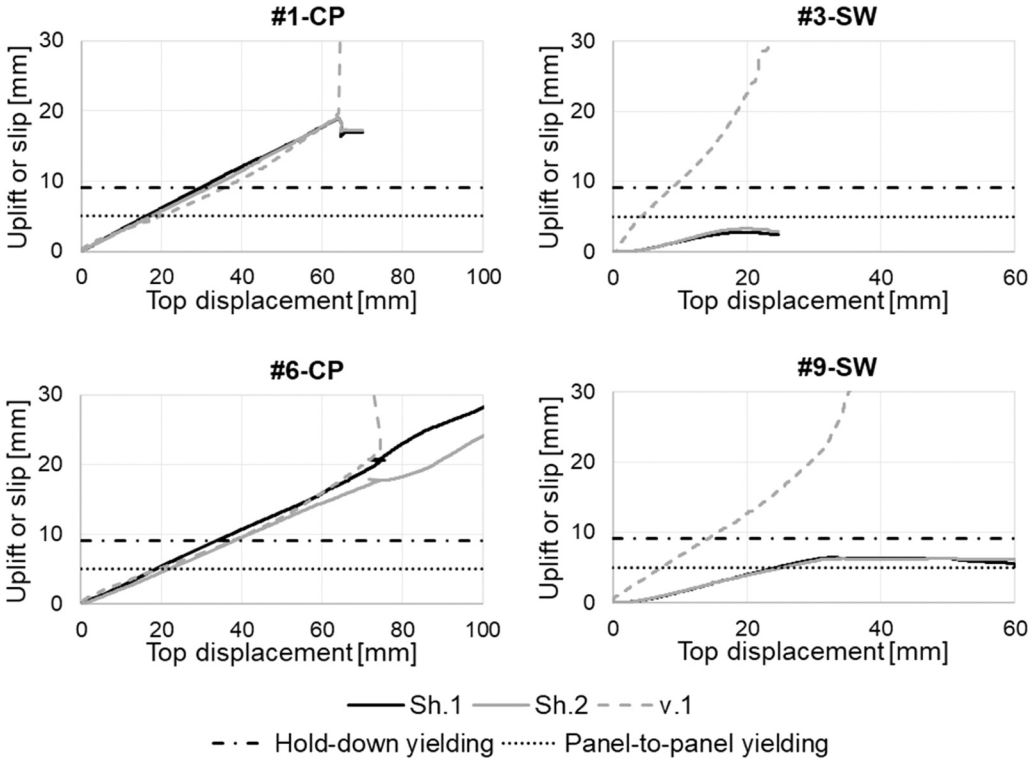


Fig. 11. Uplift of the first panel (v.1) and slips between panels (Sh.1 & Sh.2) vs top displacement.

developed only for CP behaviour.

The factored elastic strength of CLT shearwalls can be determined using Eqs. (5) and (6) for walls with CP and SW behaviour, respectively.

$$R_{w,r,CP} = \min\left(r_h \bullet \frac{k_R' \bullet b}{k_h \bullet h}; r_f \bullet \frac{k_R' \bullet b}{k_f \bullet h}\right) + \frac{q \bullet m \bullet b^2}{2 \bullet h} \tag{5}$$

$$R_{w,r,SW} = \min\left[2 \bullet r_h \bullet b \bullet m + q \bullet m^2 \bullet b^2; 2 \bullet r_f \bullet n_f \bullet b \bullet m + q \bullet b^2 \bullet \left(2 \bullet m - m^2\right)\right] \bullet \frac{1}{2 \bullet h} \tag{6}$$

where r_h and r_f are the factored resistances of the hold-down in uplift and the panel-to-panel connections in shear, respectively; k_h and k_f are

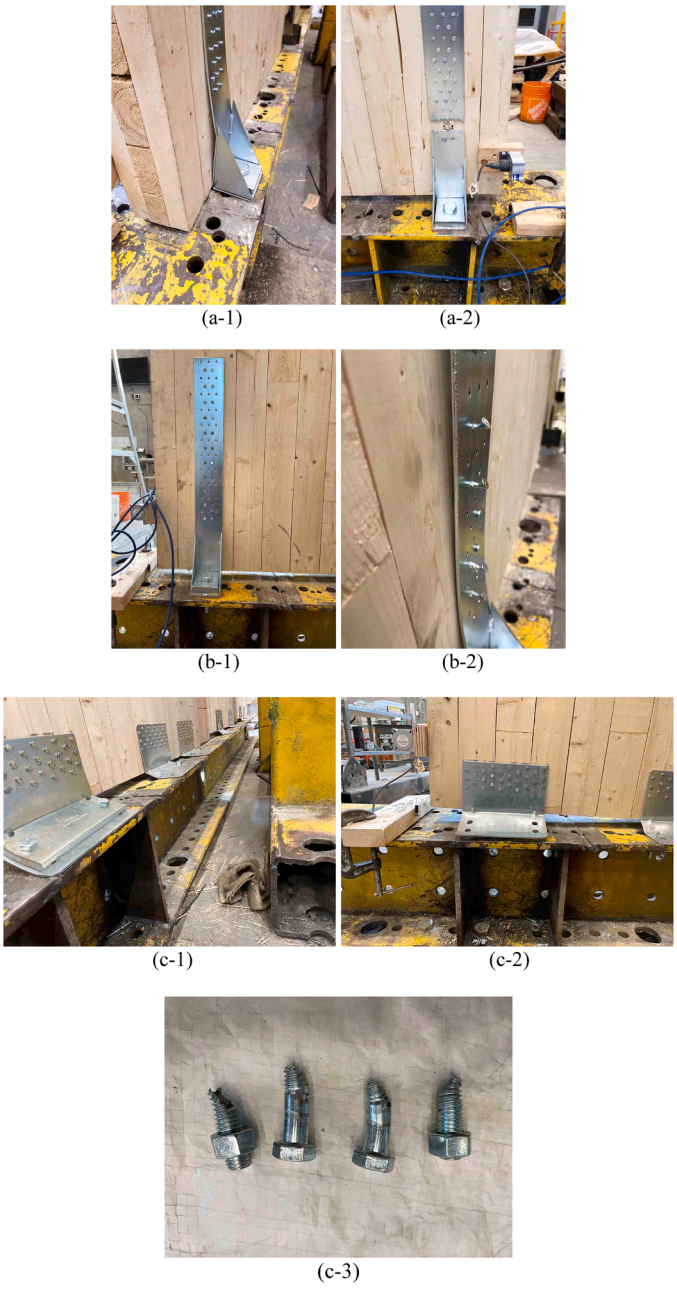


Fig. 12. (a−1 & a−2) Fully nailed hold-down before and after failure, (b−1 & b−2) partially nailed hold-down before and after failure, and (c−1, c−2 & c−3) fully nailed angle bracket with washer before and after failure.

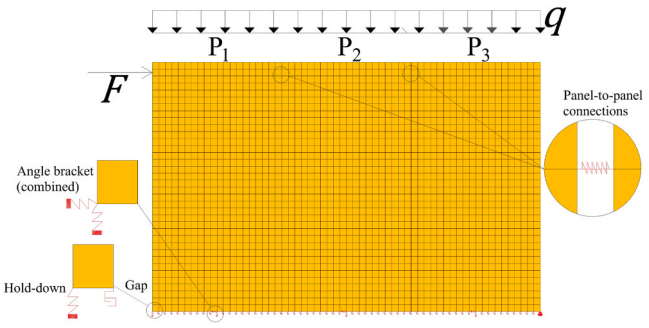


Fig. 13. Numerical model of a three-panel CLT shearwall in SAP2000.

the corresponding elastic stiffnesses of the hold-down and panel-to-panel connections; and k_R' is the equivalent hold-down stiffness for CP behaviour, obtained from Eq. (7).

$$k_R' = k_h \bullet K_U + (m-1) \bullet n_f \bullet k_f \tag{7}$$

K_U is the uplift contribution factor and can be calculated using Eq. (8).

$$K_U = 1 + \alpha \bullet \beta \bullet m \tag{8}$$

Where α and β can be determined using Eqs. (9) and (10).

$$\alpha = \frac{n_s \bullet (2 \bullet n_s + 1)}{6 \bullet (n_s + 1)} \tag{9}$$

$$\beta = \frac{k_{sz}}{k_h} \tag{10}$$

k_{sz} represents the elastic uplift stiffness of a single bracket when present.

Eq. (11) must be satisfied to ensure CP behaviour for both wall series and Eq. (12) to ensure SW behaviour for wall Serie A.

$$\widetilde{k} \geq \frac{1 - \widetilde{q} \bullet \left(\frac{3 \bullet m - 2}{m^2}\right)}{1 + \frac{\beta \bullet n_s}{2} - \widetilde{q} \bullet \left(\frac{m \bullet \left(1 + \frac{\beta \bullet n_s}{2}\right) - 2 \bullet K_U}{m^2}\right)} \tag{11}$$

$$\widetilde{k} < \frac{1 - \widetilde{q}}{1 - \widetilde{q} \bullet (m-2)} \tag{12}$$

$\widetilde{k}$ and $\widetilde{q}$ are dimensionless stiffness and load factors, determined from Eqs. (13) and (14), respectively. F denotes the factored lateral load.

$$\widetilde{k} = \frac{k_h}{n_f \bullet k_f} \tag{13}$$

$$\widetilde{q} = \frac{q \bullet m^2 \bullet b^2}{2 \bullet F \bullet h} \tag{14}$$

Elastic deflection can be determined using Eq. (15).

$$\Delta_w = \frac{F_{sp}}{k_w} - \Delta_q \tag{15}$$

where F_{sp} is the specified (unfactored) lateral load, and k_W and Δ_q represent the equivalent lateral stiffness of the CLT shearwall and the deflection due to the gravity load stabilizing impact, determined using Eqs. (16) and (17), respectively.

$$\frac{1}{k_W} = \frac{1}{k_A} + \frac{1}{k_B} + \frac{1}{k_R} + \frac{1}{k_S} \tag{16}$$

$$\Delta_q = \begin{cases} \dfrac{q \bullet m \bullet h}{2 \bullet k_R'} & \textit{for CP} \\ \dfrac{q \bullet h}{2 \bullet k_h} & \textit{for SW} \end{cases} \tag{17}$$

k_A, k_B, k_R, and k_S are the CLT shearwall stiffnesses due to wall panel shear deformation, wall panel bending deformation, rocking deformation, and sliding deformation, respectively, and can be calculated using (18)-(21).

$$k_A = \frac{G_{eff} \bullet t_{CLT} \bullet m \bullet b}{h} \tag{18}$$

$$k_B = \frac{3 \bullet EI_{eff}}{h^3} \tag{19}$$

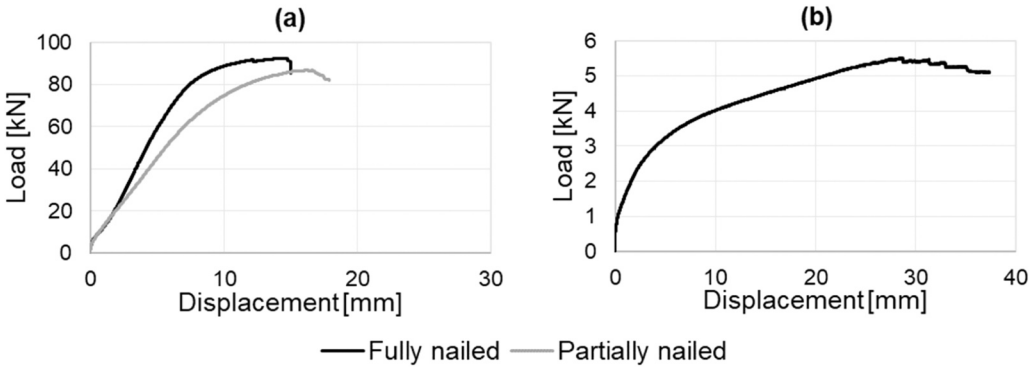


Fig. 14. The average load-displacement envelope curves of: (a) fully- and partially nailed WHT620 hold-downs under uplift (b) HBS 6 × 70 mm fasteners under shear.

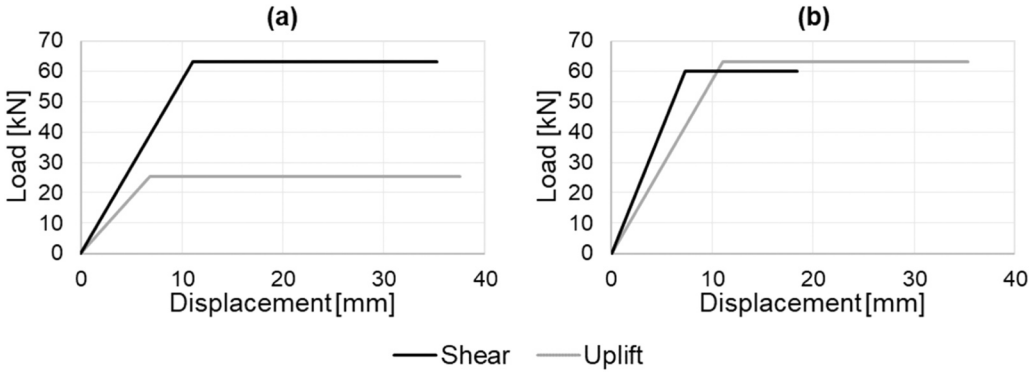


Fig. 15. The average bi-linear load-displacement curves of TCN200 angle brackets (a) without washer (b) with washer.

$$k_R = \begin{cases} \dfrac{k_R' \bullet b^2}{h^2} & for\ CP \\ \dfrac{b^2 \bullet m^2}{h^2} \bullet \left(\dfrac{1}{k_h} + \dfrac{m-1}{n_f \bullet k_f}\right)^{-1} & for\ SW \end{cases} \tag{20}$$

$$k_S = k_{sx} \bullet m \bullet n_s \tag{21}$$

where k_{sx} is the stiffness of each angle bracket at the base of the shearwall in sliding (horizontal shear), which is set to zero for Series A since no angle brackets were used. EI_{eff} can be obtained using Eq. (22).

$$EI_{eff} = \frac{m \bullet b^3}{12} \bullet \left(t_{CLT,V} \bullet E_0 + t_{CLT,H} \bullet E_{90}\right) \tag{22}$$

where $t_{CLT,V}$ and $t_{CLT,H}$ are the total thicknesses of the vertical (70 mm) and horizontal layers (35 mm) of the CLT wall panels, respectively.

Based on the capacity-based design principle for CLT shearwalls, the panel-to-panel connections must yield first, followed by hold-down yielding. To ensure this sequence, Eq. (23) must be satisfied. $r_{f,peak,15}$ represents the 15th-percentile peak resistance of the panel-to-panel connections. Note that the expression for $\tilde{k} \geq 1$ is applicable to both Series A and B, whereas that for $\tilde{k} < 1$ is only applicable to Series A, since it represents an elastic kinematic behaviour other than CP.

$$\begin{cases} r_{h,peak} \geq r_{f,peak,15} \bullet \dfrac{k_h}{k_f} & when\ \tilde{k} \geq 1 \\ r_{h,peak} \geq \max\left(r_{f,peak,15} \bullet \dfrac{k_h}{k_f}; n_f \bullet r_{f,peak,15} - q \bullet b\right) & when\ \tilde{k} < 1 \end{cases} \tag{23}$$

According to Ref. [29], values for $r_{f,peak,15}$ can be taken as $\gamma_{rh} \bullet r_{f,peak}$, where γ_{rh} is the corresponding over-strength factor equal to 1.3. $r_{h,peak}$ and $r_{f,peak}$ are the peak resistances of the hold-down and panel-to-panel connections, respectively.

For the walls that satisfy the sequence of yielding (i.e. panel-to-panel connections yield before the hold-down), the factored rocking plastic resistance of CLT shearwalls under seismic loads, $R_{s,r}$, can be obtained using Eq. (24). Eq. (25) is used to calculate the factored rocking moment resistance of the shearwall under seismic, M_{sr}.

$$R_{s,r} = \frac{M_{sr}}{h} \tag{24}$$

$$M_{sr} = b \bullet \left[r_{h,peak} \bullet K_U + r_{f,peak} \bullet (m-1) \bullet n_f + \frac{q \bullet m \bullet b}{2}\right] \tag{25}$$

5.1. Analytical model: findings and discussion

Table 7 presents the mechanical properties of the connections used in each test, as reported in Ref. [29], including elastic and yield parameters derived from the EEEP curves. Walls #9 and #10 were excluded from the comparison because no expressions are provided in Ref. [1] for walls with SW behaviour with uplift contribution from angle brackets. For wall #8, where fully nailed (30 nails) TCN200 angle brackets with thick washer were used instead of hold-down at the wall ends, the uplift stiffness and resistance were obtained by calibrating the properties reported in Ref. [29] for partially nailed (20 nails) brackets in proportion to the number of nails, since the uplift performance is primarily related to the strength and stiffness of the nails in the TCN200 angle brackets with washers.

Table 8 presents the results obtained from the analytical expressions. CP and SW checks were performed for each wall based on the mode observed in the tests. For the CD yield hierarchy, the requirement that the hold-downs yield after vertical joints was satisfied, which is in agreement with the test results presented in the experimental results

Table 6
results obtained from experimental tests and numerical models.

Wall-mode	Content	F_{max} [kN]	$v_{F_{max}}$ [mm]	$F_{y,EEEP}$ [mm]	$v_{y,EEEP}$ [mm]	$k_{e,EEEP}$ [kN/mm]	v_u [mm]	D_{EEEP} [-]
#1-CP	Test	130.1	53.0	115.5	23.4	4.9	64.1	2.7
	Numerical	125.0	50.4	110.1	24.0	4.2	50.5	2.1
	$\xi_{T/N}$	4.0%	5.1%	4.8%	2.7%	16.2%	23.7%	26.3%
#2-CP	Test	146.4	49.3	134.3	29.4	4.6	58.3	2.0
	Numerical	141.4	48.7	126.5	21.4	5.4	51.2	2.4
	$\xi_{T/N}$	3.5%	1.3%	6.0%	31.7%	16.6%	13.0%	19.1%
#3-SW	Test	120.3	17.7	109.5	11.8	9.3	20.8	1.8
	Numerical	127.0	17.2	114.2	10.9	10.5	19.1	1.8
	$\xi_{T/N}$	5.4%	3.0%	4.2%	7.5%	11.7%	8.5%	1.1%
#4-SW	Test	145.3	23.0	126.0	11.7	10.8	24.1	2.1
	Numerical	143.2	19.1	126.6	11.0	10.7	19.8	1.8
	$\xi_{T/N}$	1.5%	18.5%	0.5%	6.1%	1.0%	19.7%	13.6%
#5-SW	Test	162.3	40.7	140.7	19.0	7.4	41.1	2.2
	Numerical	160.5	35.8	138.6	12.6	10.4	35.8	2.8
	$\xi_{T/N}$	1.1%	12.7%	1.5%	40.5%	33.7%	13.8%	27.2%
#6-CP	Test	164.0	73.1	146.1	38.6	3.8	74.4	1.9
	Numerical	160.8	55.1	142.3	30.8	4.2	55.4	1.8
	$\xi_{T/N}$	1.9%	28.1%	2.6%	22.4%	10.3%	29.3%	7.0%
#7-CP	Test	172.3	65.7	147.4	31.1	4.8	67.6	2.2
	Numerical	165.3	55.4	146.8	31.1	4.5	55.8	1.8
	$\xi_{T/N}$	4.2%	17.0%	0.4%	0.1%	5.4%	19.2%	19.4%
#8-CP	Test	140.1	70.8	120.6	25.4	4.8	84.9	3.3
	Numerical	163.0	69.9	139.5	30.0	4.4	69.9	2.3
	$\xi_{T/N}$	15.1%	1.2%	14.6%	16.6%	7.7%	19.4%	35.6%
#9-SW	Test	164.7	31.5	145.5	19.6	7.4	34.5	1.8
	Numerical	173.8	30.8	147.9	18.2	7.8	30.8	1.7
	$\xi_{T/N}$	5.4%	2.4%	1.7%	7.3%	4.9%	11.2%	3.9%
#10-SW	Test	189.5	33.6	161.8	15.5	10.4	36.0	2.3
	Numerical	199.9	38.0	166.0	18.3	8.5	38.0	2.1
	$\xi_{T/N}$	5.4%	12.3%	2.6%	16.4%	20.3%	5.3%	11.1%
#11-CP	Test	120.1	55.5	112.1	37.2	3.0	60.2	1.6
	Numerical	119.4	56.9	109.4	32.6	3.1	57.4	1.8
	$\xi_{T/N}$	0.6%	2.4%	2.5%	13.3%	2.9%	4.7%	8.3%
#12-CP	Test	76.5	118.0	71.9	78.6	0.9	144.9	1.8
	Numerical	74.2	117.2	63.2	50.9	1.1	117.7	2.3
	$\xi_{T/N}$	3.1%	0.7%	12.9%	42.8%	17.8%	20.7%	22.8%
$\xi_{T/N}$	Maximum	15.1%	28.1%	14.6%	42.8%	33.7%	29.3%	35.6%
	Minimum	0.6%	0.7%	0.4%	0.1%	1.0%	4.7%	1.1%
	Mean	4.3%	8.7%	4.5%	17.3%	12.4%	15.7%	16.3%

Table 7
Mechanical properties of connections used in analytical comparisons and derived from EEEP curves.

Variable	Unit	#1 & #2	#3 & #4	#5	#6 & #7	#8	#11	#12
k_h	kN/mm	22.4	8.6	11.2	22.4	8.2	22.4	22.4
k_f	kN/mm	1.0	1.0	1.0	1.0	1.0	1.0	1.0
k_{sz}	kN/mm	-	-	-	4.4	4.4	4.4	4.4
k_{sx}	kN/mm	-	-	-	6.2	6.2	6.2	6.2
r_h	kN	178.4	81.4	89.2	178.4	88.8	178.4	178.4
r_f	kN	4.8	4.8	4.8	4.8	4.8	4.8	4.8
r_{sz}	kN	-	-	-	25.4	25.4	25.4	25.4
n_s	-	0	0	0	2	2	2	1
n_f	-	9	35	26	9	9	9	9

section and in Fig. 11. This agreement between analytical predictions and experimental observations confirms the applicability of the analytical expressions for predicting both the governing kinematic mode and the yield hierarchy.

Table 9 summarizes the experimental reference parameters used for comparison along with deviations for each of these three quantities.

For elastic strength, the deviation ranges from + 9% to + 12% for SW walls, indicating a slight overestimation, while CP behaviour exhibited an underestimation of −11% to −28%, which is considered reasonable given the assumptions made to define the connection yield strength and the inherent variability of timber and steel connection properties [29]. For elastic deflection, the deviation is between −29% and + 28% for walls #1-#7 and #11. Wall #8 shows a larger deviation of + 35%, mainly related to the assumptions adopted to define the properties of the angle brackets with washers. Wall #12 exhibits an even larger deviation (−77%), indicating that the analytical model substantially underestimated the experimental deflection. This behaviour is consistent with its slender geometry (aspect ratio 4:1) and greater number of panels, which make the global response more sensitive to panel bending deformations. Additional discrepancies may arise from the use of the EEEP idealization for panel-to-panel connections, whereas a significantly better fit was obtained in the numerical model when the full connection curves from the joint-level tests were used.

For plastic strength, the deviation ranges from + 2% to + 20% for all walls except wall #8. For wall #8, the deviation increases to + 29%, again reflecting the uncertainties associated with the assumed angle bracket properties. It is also important to note that, in the code expressions, the hold-downs are located exactly at the wall ends and the

Table 8
The analytical results.

	$R_{w,r}$	$\Delta_{w,F=35kN}$	CP check	SW check	CD yielding	$M_{s,r}$	$R_{s,r}$
Eq.	(5),(6)	(15)	(11)	(12)	(23)	(25)	(24)
Unit	[kN]	[mm]	[-]	[-]	[-]	[kN•m]	[kN]
#1	87.7	4.4	2.49>0.97 ✔	-	186.8>163.1 ✔	354.1	145.1
#2	103.1	3.9	2.49>0.88 ✔	-	186.8>163.1 ✔	365.8	149.9
#3	126.1	3.6	-	0.25<1.00 ✔	88.0 < 253.0 ×	-	-
#4	140.4	2.8	-	0.25<1.00 ✔	88.0 < 246.7 ×	-	-
#5	152.1	2.9	-	0.43<1.00 ✔	93.4 < 181.1 ×	-	-
#6	113.9	5.0	2.49>0.67 ✔	-	186.8>163.1 ✔	420.2	172.2
#7	118.7	4.5	2.49>0.61 ✔	-	186.8>163.1 ✔	431.9	177.0
#8	99.5	5.0	1.82>0.63 ✔	-	195.6>119.4 ✔	459.4	188.3
#11	86.6	7.0	2.49>0.56 ✔	-	186.8>163.1 ✔	335.6	137.6
#12	64.4	15.5	2.49>0.80 ✔	-	186.8>163.1 ✔	227.1	93.1

Table 9
The comparison between experimental tests and analytical models.

	$F_{y,tri}$	$R_{w,r}$	Dev.	v_{35kN}	$\Delta_{w,F=35kN}$	Dev.	F_{max}	$R_{s,r}$	Dev.
Unit	kN	kN	(%)	mm	mm	(%)	kN	kN	(%)
#1	109.9	87.7	−22%	3.8	4.4	+14%	130.1	145.1	+11%
#2	136.1	103.1	−28%	5.3	3.9	−29%	146.4	149.9	+2%
#3	111.3	126.1	+12%	3.2	3.6	+12%	-	-	-
#4	127.5	140.4	+10%	2.5	2.8	+11%	-	-	-
#5	139.2	152.1	+9%	2.7	2.9	+6%	-	-	-
#6	146.7	113.9	−25%	5.0	5.0	0%	164.0	172.2	+5%
#7	147.7	118.7	−22%	3.4	4.5	+28%	172.3	177.0	+3%
#8	120.5	99.5	−19%	3.5	5.0	+35%	140.1	188.3	+29%
#11	112.1	86.6	−26%	8.5	7.0	−20%	120.1	137.6	+14%
#12	71.9	64.4	−11%	34.9	15.5	−77%	76.5	93.1	+20%

angle brackets are equally distributed along each panel length. In the experimental tests, however, the hold-downs were installed slightly away from the panel edges, and the angle brackets were slightly misaligned from their analytical locations. These discrepancies may also have affected the results and contributed to the deviations.

To quantify the efficiency of the VJ in providing joint rigidity, the rocking stiffness of each wall, k_R, calculated using Eq. (20), is compared with two reference cases: (i) $k_{R,b}$, where the panel-to-panel connection stiffness is set to zero and only the first panel with the length of b is considered, with the hold-down and angle brackets (for wall Series B) contributes to the rocking stiffness; (ii) $k_{R,B}$, where the panel-to-panel connections are assumed rigid and a single wall with total length of B is considered, with the hold-down and all angle brackets along the wall length contributing to the rocking stiffness. Table 10 summarizes the corresponding stiffness values for all three cases, together with the efficiency factor $\xi_{R,e}$ defined in Eq. (26). As can be seen, the loss of rocking stiffness for CP walls is significant, with efficiencies in the range of 7–12%, which is consistent with the high flexibility of the panel-to-panel connections. In contrast, SW walls exhibit efficiencies in the range between 48% and 63%, indicating a response closer to that of a single-panel wall and, therefore, stiffer panel-to-panel connections. Overall, these results confirm that CP walls exhibit much greater rocking flexibility, whereas SW walls are comparatively stiffer and less sensitive to VJ flexibility. The influence of key parameters, including wall geometry, gravity loads, and mechanical properties of connections, on the lateral behaviour of multi-panel CLT shearwalls is systematically investigated and discussed in Ref. [16].

Table 10
Rocking stiffness efficiency comparison.

	Kinematic mode	k_R	$k_{R,b}$	$k_{R,B}$	$\xi_{R,e}$
Unit	-	kN/mm	kN/mm	kN/mm	%
#1	CP	10.1	5.6	50.4	10%
#2	CP	10.1	5.6	50.4	10%
#3	SW	13.0	2.15	19.3	63%
#4	SW	13.0	2.15	19.3	63%
#5	SW	13.5	2.8	25.2	48%
#6	CP	11.7	6.1	66.7	9%
#7	CP	11.7	6.1	66.7	9%
#8	CP	10.2	4.6	53.2	11%
#11	CP	8.9	6.1	29.6	12%
#12	CP	3.3	1.5	29.6	7%

$$\xi_{R,e} = \frac{k_R - k_{R,b}}{k_{R,B} - k_{R,b}} \tag{26}$$

6. Conclusions

This paper provides a comprehensive investigation into the performance of single-storey multi-panel CLT shearwalls subjected to lateral loads. The conclusions drawn from study can be summarized as follows:

- Walls displaying SW behaviour exhibited nearly double the stiffness compared to those with CP behaviour, while the ultimate displacement was significantly lower, highlighting that kinematic mode selection has a fundamental influence on both the stiffness and deformation capacity in CLT shearwall design.
- In CP mode, panel-to-panel connections yielded prior to hold-downs, while SW mode walls maintained elastic connections throughout the tests until hold-downs eventually yielded. Ductility ratios ranged from 2.0 to 2.9 for CP behaviour and approximately 1.7–2.3 for SW behaviour. The comparable ductility ratios between the two modes are attributed to the connections engagement mechanism. In CP, hold-down failure intervenes before panel-to-panel connections fully exploit their deformation capacity, while in SW, residual panel-to-panel flexibility enhanced the wall lateral behaviour governed by the hold-down. This has direct implications for the refinement of capacity-based design approaches targeting specific ductility levels in seismic applications.
- Employing a greater number of panels, while maintaining the same wall length, resulted in decreased resistance and stiffness while slightly enhancing the ductility. This highlights the importance of

identifying an optimal wall panel configuration to achieve the desired balance between resistance and ductility in design.

- Walls incorporating angle brackets demonstrated significantly higher resistance, resulting in approximately 26% and 37% resistance increases for CP and SW behaviour walls, respectively. This indicates that even angle brackets of moderate stiffness installed near the middle of each panel can still contribute substantially to the uplift resistance of the wall.
- Ultimate failure consistently occurred in hold-down connections due to their lower ultimate displacement compared to panel-to-panel connections, consistent with connection-level tests presented in the literature and emphasizing the importance of the hold-down as the critical element in capacity-based design considerations.
- The inclusion of gravity loads led to notably greater maximum resistance, while having negligible effects on other properties, including elastic stiffness and ductility, suggesting that gravity load contributions can be reliably incorporated into design resistance expressions without significant impact on ductility-based design assumptions.
- Numerical models achieved reasonable agreement for all wall specimens, accurately capturing elastic stiffness, plastic behaviour, and Kinematic modes for both CP and SW behaviour walls, demonstrating the suitability of simplified models as practical design-oriented tools.
- Comparisons between analytical predictions and experimental results confirmed that the analytical expressions can accurately identify the kinematic mode (CP or SW) and reliably capture the yield hierarchy required for capacity design, supporting their applicability across different geometries, connection layouts, and gravity load conditions, including those adopted in CSA O86–24.
- The analytical expressions from the literature and CSA O86–24 standard showed reasonable agreement with the experimental results, contributing to the validation of recently introduced design expressions against a broader range of wall configurations than previously tested.
- Multi-panel CP walls exhibited much greater rocking flexibility (7–12% efficiency), while SW walls remained comparatively stiff (48–63%), indicating lower sensitivity to vertical joint flexibility.

Future efforts will focus on conducting experimental tests on multi-panel, multi-storey CLT shearwalls to investigate the contribution of connections under cyclic loading and their impact on global response, as well as on developing analytical expressions for multi-storey applications with various floor-to-wall connections involved in the lateral behaviour of platform-type CLT shearwalls.

CRediT authorship contribution statement

Daniele Casagrande: Writing – review & editing, Validation, Supervision, Methodology, Conceptualization. **Ghasan Doudak:** Writing – review & editing, Supervision, Project administration, Conceptualization. **Mohammad Masroor:** Writing – review & editing, Writing – original draft, Visualization, Validation, Software, Methodology, Investigation, Formal analysis, Data curation, Conceptualization.

Declaration of Competing Interest

As first author and corresponding author, I declare that there is no conflict of interest for the original research paper entitled "*An Experimental Investigation of multi-panel Cross-Laminated Timber shearwalls*", by M. Masroor, G. Doudak, D. Casagrande.

Acknowledgements

The authors wish to extend their sincere appreciation to Rothoblaas Srl (Italy) and Nordic Structures (Canada) for their invaluable support in supplying the connections and CLT panels utilized in this investigation.

Data availability

Data will be made available on request.

References

[1] CSA O86-24, Engineering design in wood. CSAO86:24, CSA Group, Mississauga, ON, Canada, 2024.
[2] A. Ceccotti, C. Sandhaas, M. Okabe, M. Yasumura, C. Minowa, N. Kawai, SOFIE project - 3D shaking table test on a seven-storey full-scale cross-laminated timber building, Earthq. Eng. Struct. Dyn. 42 (13) (2013) 2003–2021, https://doi.org/10.1002/eqe.2309.
[3] V. Hristovski, V. Mircevska, B. Dujic, M. Garevski, Comparative dynamic investigation of cross-laminated wooden panel systems: shaking-table tests and analysis, Adv. Struct. Eng. 21 (10) (2018) 1421–1436, https://doi.org/10.1177/1369433217749766.
[4] M. Lauriola, C. Sandhaas, Quasi-Static and Pseudo-Dynamic Tests on XLAM Walls and Buildings. International Workshop on "Earthquake Engineering on Timber Structures, COST Action E29, Coimbra, Portugal, 2006, pp. 119–133.
[5] A. Ceccotti, M. Follesa, Seismic Behaviour of Multi-Storey XLam Buildings. International Workshop on "Earthquake Engineering on Timber Structures, COST Action E29, Coimbra, Portugal, 2006, pp. 81–95.
[6] G. Flatscher, G. Schickhofer, Shaking-table test of a cross-laminated timber structure, Proc. Inst. Civil. Eng. - Struct. Build. 168 (11) (2015) 878–888, https://doi.org/10.1680/stbu.13.00086.
[7] M. Popovski, I. Gavric, Performance of a 2-story CLT house subjected to lateral loads, J. Struct. Eng. 142 (4) (2016), https://doi.org/10.1061/(ASCE)ST.1943-541X.0001315.
[8] M. Popovski, J. Schneider, M. Schweinsteiger, Lateral load resistance of cross-laminated wood panels, World Conference on Timber Engineering (WCTE), Riva del Garda, Italy (2010).
[9] I. Gavric, M. Fragiacomo, A. Ceccotti, Cyclic behavior of CLT wall systems: experimental tests and analytical prediction models, J. Struct. Eng. 141 (11) (2015) 04015034, https://doi.org/10.1061/(ASCE)ST.1943-541X.0001246.
[10] G. Flatscher, K. Bratulic, G. Schickhofer, Experimental tests on cross-laminated timber joints and walls, Proc. Inst. Civil. Eng. - Struct. Build. 168 (11) (2015) 868–877, https://doi.org/10.1680/stbu.13.00085.
[11] V. Hristovski, B. Dujic, M. Stojmanovska, V. Mircevska, Full-scale shaking-table tests of XLam panel systems and numerical verification: specimen 1, J. Struct. Eng. 139 (11) (2013) 2010–2018, https://doi.org/10.1061/(ASCE)ST.1943-541X.0000754.
[12] S. Dires, T. Tannert, Performance of coupled CLT shear walls with internal perforated steel plates as vertical joints and hold-downs, Constr. Build. Mater. 346 (2022) 128389, https://doi.org/10.1016/j.conbuildmat.2022.128389.
[13] A. Polastri, D. Casagrande, Mechanical behaviour of multi-panel cross laminated timber shear-walls with stiff connectors, Constr. Build. Mater. 332 (2022) 127275, https://doi.org/10.1016/j.conbuildmat.2022.127275.
[14] G. Flatscher, G. Schickhofer, Displacement-based determination of laterally loaded Cross Laminated Timber (CLT) wall systems. INTER - International Network on Timber Engineering Research [INTER/49-12-1], Timber Scientific Publishing, Graz, Austria, 2016.
[15] A. Aloisio, F. Boggian, H.Ø. Sævareid, J. Bjørkedal, R. Tomasi, Analysis and enhancement of the new Eurocode 5 formulations for the lateral elastic deformation of LTF and CLT walls, Structures 47 (2023) 1940–1956, https://doi.org/10.1016/j.istruc.2022.11.129.
[16] M. Masroor, G. Doudak, D. Casagrande, The effect of bi-axial behaviour of mechanical anchors on the lateral response of multi-panel CLT shearwalls, Eng. Struct. 224 (2020), https://doi.org/10.1016/j.engstruct.2020.111202.
[17] D. Casagrande, G. Doudak, A. Polastri, A proposal for the capacity-design at wall- and building-level in light-frame and cross-laminated timber buildings, Bull. Earthq. Eng. 17 (6) (Jun. 2019) 3139–3167, https://doi.org/10.1007/s10518-019-00578-4.
[18] M. Masroor, G. Doudak, D. Casagrande, Design of multipanel CLT shear walls with bidirectional mechanical anchors following capacity-based design principle, J. Perform. Constr. Facil. 36 (1) (2022), https://doi.org/10.1061/(ASCE)CF.1943-5509.0001693.
[19] M. Masroor, M. Gheisari, T. Tannert, Experimental parameter study of two-story platform-type CLT shear walls, J. Struct. Eng. 150 (8) (2024), https://doi.org/10.1061/JSENDH.STENG-13277.
[20] G. D'Arenzo, S. Schwendner, W. Seim, The effect of the floor-to-wall interaction on the rocking stiffness of segmented CLT shear-walls, Eng. Struct. 249 (2021) 113219, https://doi.org/10.1016/j.engstruct.2021.113219.
[21] G. D'Arenzo, W. Seim, M. Fossetti, Experimental characterization of a biaxial behaviour connector for CLT wall-to-floor connections under different load directions, Constr. Build. Mater. 295 (2021) 123666, https://doi.org/10.1016/j.conbuildmat.2021.123666.
[22] M. Masroor, D. Casagrande, T. Tannert, G. Doudak, Analytical model for lateral deflection of multi-storey platform-type CLT shear walls accounting for floor-wall interaction, J. Build. Eng. 115 (2025) 114587, https://doi.org/10.1016/j.jobe.2025.114587.
[23] ANSI/APA, ANSI/APA PRG 320:2019 standard for performance-rated cross-laminated timber, APA- The Engineered Wood Association (2020).

[24] ETA-11/0086, RothoBlaas WHT hold downs and angle brackets, European Organization for Technical approval, Denmark, 2018.
[25] ETA-11/0496, "RothoBlaas TITAN Angle Brackets," Denmark, 2014.
[26] ETA-11/0030, RothoBlaas Self-tapping screws and threaded rods, European Organization for Technical approval, Denmark, 2019.
[27] ASTM E2126, "Standard test methods for cyclic (reversed) load test for shear resistance of vertical elements of the lateral force resisting systems for buildings," West Conshohocken, PA, 2019.
[28] EN 12512, *Timber structures - Test methods - Cyclic testing of joints made with mechanical fasteners*. 2005.
[29] Mohammad Masroor, Multi-Panel CLT Shearwalls: Experimental Assessment, Analytical Development, and Design Considerations, University of Ottawa, Ottawa, 2023, https://doi.org/10.20381/ruor-29134.
[30] CSI, SAP2000 Integrated Software for Structural Analysis and Design, Computers and Structures Inc., Berkeley, California, 2018, p. 18.
[31] R. Brandner, P. Dietsch, J. Dröscher, M. Schulte-Wrede, H. Kreuzinger, M. Sieder, Cross laminated timber (CLT) diaphragms under shear: test configuration, properties and design, Constr. Build. Mater. 147 (2017) 312–327, https://doi.org/10.1016/j.conbuildmat.2017.04.153.
[32] M. Masroor, G. Doudak, D. Casagrande, Experimental investigation of dissipative connections in cross-laminated timber shearwalls, Constr. Build. Mater. 413 (2024) 134828, https://doi.org/10.1016/j.conbuildmat.2023.134828.
[33] G. D'Arenzo, D. Casagrande, A. Polastri, M. Fossetti, M. Fragiacomo, W. Seim, CLT shear walls anchored with shear-tension angle brackets: experimental tests and finite-element modeling, J. Struct. Eng. 147 (7) (2021), https://doi.org/10.1061/(ASCE)ST.1943-541X.0003008.